Winding Optimization for Reducing Parasitic Capacitances of Common-Mode Chokes

Pablo Ruiz-Morales, Álvaro Ojeda-Rodríguez, Joaquín Bernal-Méndez, *Senior Member, IEEE*, and María A. Martín-Prats, *Senior Member, IEEE*

***Abstract*—Parasitic capacitances typically undermine the filtering performance of common mode chokes at high frequencies. This work demonstrates that these parasitic capacitances can be reduced by using a wise winding strategy that depends on the physical properties of the core material. Due to its practical interest, we specifically focus on single-layer common mode chokes wounded on NiZn or MnZn ferrite cores. Based on a physical model that enables the identification of parameters influencing the electrical coupling between the turns of the coils of the choke, the hypothesis proposed is that the optimal winding configuration depends on the core material, differing for NiZn and MnZn cores. To verify this hypothesis and to assess improvements actually achieved by optimum winding strategies, an accurate high-frequency model of the common mode choke along with an efficient characterization technique are used to numerically estimate the parasitics of common-mode chokes with different core materials and winding configurations. In addition, the filtering performance of these common mode chokes have been measured and compared.**

***Index Terms*—Common mode chokes (CMC), design of inductors, electromagnetic interference (EMI), EMI filters, parasitic capacitance.**

I. Introduction

RECENT advances in semiconductor device technology and design techniques have led to an upward trend in the switching frequencies of power electronic devices, driven by the objective of increasing power density [1]. However, this increase in switching frequencies comes with an inevitable increment in the frequency content of the spectrum of conducted and radiated noise emissions, which can cause a wide range of electromagnetic compatibility (EMC) problems [2]. Due to this, specific design and mitigation strategies are typically used to help to comply with the EMC normative applicable in different technological fields [3]. In most cases, these EMC-conscious design strategies must be complemented with the use of electromagnetic interference (EMI) filters [2], [3].

Manuscript received 23 January 2024; revised 26 March 2024; accepted 18 April 2024. This work was supported under Grant TED2021-131954B-I00 funded by MCIN/AEI/10.13039/501100011033 and in part by the European Union NextGenerationEU/PRTR. *(Corresponding author: Pablo Ruiz Morales.)*

Pablo Ruiz-Morales, Álvaro Ojeda-Rodríguez, and María A. Martín-Prats are with the Department of Electronic Engineering, University of Seville, 41004 Sevilla, Spain (e-mail: pruiz4@us.es).

Joaquín Bernal-Méndez is with the Department of Applied Physics III, University of Seville, 41004 Sevilla, Spain.

Color versions of one or more figures in this article are available at https://doi.org/10.1109/TEMC.2024.3395800.

Digital Object Identifier 10.1109/TEMC.2024.3395800

In many EMI filters, common-mode chokes (CMC) are used to attenuate common-mode (CM) emissions. A CMC consists of two tightly coupled coils typically wounded on a toroidal core [2]. The idea of the CMC is to present a high inductive impedance to CM noise while at the same time avoiding saturation due to the functional differential-mode (DM) currents. For this reason, CMCs are ideally transparent to DM noise, although a small leakage inductance is typically allowed to aid in the attenuation of high-frequency DM noise [2], [4]. Although the response of a CMC is mainly inductive in the low frequency range, its effectiveness as a filtering device is undermined at high frequencies by capacitive parasitic effects, which are caused by displacement currents through the air and through the core of the CMC [5]. Countermeasures required to compensate for this underperformance of the CMC typically require the addition of additional filtering components, which causes a negative impact on the cost and weight of the final design that might not be assumable, especially in certain applications [6], [7].

Due to the problem posed by parasitic capacitances in inductive filtering components, various works in the literature focus on estimating the equivalent parasitic capacitance (EPC) for inductors or for specific connections of a CMC [5], [8], [9], [10], [11]. These studies demonstrate that EPC generally has a contribution arising from the electrical coupling between turns of the inductor and another contribution associated with the coupling of turns to the core. These concepts are used in Dong et al.'s [12] work to develop an analytical method for estimating the parasitic capacitances affecting a CMC in both CM and DM. However, this study is only applied to a specific CMC with a nanocrystalline core, and an investigation into the impact of key parameters, such as core permittivity or winding arrangement on the capacitive effects measured in that CMC is not conducted. Recently, in Li and Wang's [13] work, the impact of the number of turns on the EPC of a single-layer inductor with a high-permittivity ring-core is analyzed, and an interesting method is proposed to reduce the EPC of the inductor by using stacked cores. In Salomez et al.'s [14] work, a model is proposed to estimate the EPC of single-layer inductors with high-permittivity ring cores. The impact of winding technique is analyzed, and it is concluded that since in this case the EPC is dominated by the electrical coupling of turns to the core, the EPC can be reduced by using tight winding or by increasing the distance between turns and the core. By contrast, in Ayachit and Kazimierczuk's [15] work, it is demonstrated that a loose winding reduces the EPC of single-layer air-core inductors.

This result is intuitive because electric coupling is generally expected to decrease with distance between coupled conductors. The apparent contradiction with the conclusions reported in Salomez et al.'s [14] work, serves to emphasize the key impact that the permittivity of the core has on the capacitive response that inductive components exhibit at high frequencies.

The aforementioned works focus on inductors with air cores or with very high permittivity cores. Therefore, these previous studies do not allow elucidating which winding strategy is optimal for other core materials with practical interest and whose typical permittivities are much lower than those of MnZn or nanocrystalline materials, such as NiZn ferrites [13]. In addition, a CMC is inherently a more complex component than an inductor. In fact, it is a four-port device with different electric field distributions for CM and DM excitations (in this case, for example, the capacitance between windings plays a role). Therefore, when studying the effect of different winding strategies, it is necessary to analyze the CM and DM response of the CMC, rather than treating it as a simple inductor.

In this study, our primary objective is to validate the hypothesis that the optimal winding configuration, with regard to the reduction of the EPC of single-layer CMCs, depends upon the core's permittivity. Consequently, this configuration may differ for materials with high permittivity, such as nanocrystalline or MnZn ferrites, compared to materials, such as NiZn ferrites. Furthermore, we aim to quantify the impact of different winding strategies on the parasitic elements of a highly accurate and wideband circuit model of the CMC proposed in Ojeda-Rodríguez et al.'s [16] work, measuring and studying their effect on the attenuation provided by the CMC, both against CM and DM noise.

The rest of this article is organized as follows. Section II presents an analysis of the effect of electric couplings on the performance of CMCs, and its dependence on the permittivity of the core. In addition, the circuit model and measurement technique that will be used to evaluate the effect of different winding configurations are discussed and employed to analyze conditions to ensure optimal performance of a CMC. Section III gathers the results of the measurements carried out to corroborate the conclusions reached in the previous section and to quantify the effect of optimal winding strategies. Finally, Section IV concludes this article.

II. Analysis

Fig. 1 schematically represents the different contributions to the electrical coupling between two turns of the windings of a CMC. In this figure, the capacitor C_{tt} accounts for direct electrical coupling through the air, while the series combination of C_{tc} and C_{cc} indicates an alternative coupling path through the core material, which encompasses the coupling of each of the two windings to the core through air (C_{tc}) and the coupling through the interior of the core (C_{cc}). As shown in Fig. 1, the parasitic capacitance C_{cc} can be considered as a capacitor filled with a dielectric material with permittivity ε. For materials with high permittivity, this capacitance will be very large ($C_{cc} \gg C_{tc}$). In this case, the coupling through the core would be determined

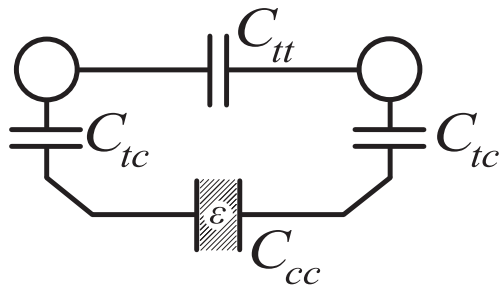

Fig. 1. Schematic representation of the electric coupling mechanisms between two turns of a winding on a magnetic ring-core.

solely by C_{tc}. This approximation is assumed by works that treat the core as a conductive material when calculating parasitic capacitances of inductors and CMCs [5], [9], [11], [12], [14]. For single-layer windings on high-permittivity materials, the coupling C_{tc} could also be a dominant effect over C_{tt} in determining the total electrical coupling between windings [13], [14]. Since C_{tc} tends to increase for loose windings [10], this winding strategy increases the EPC of inductors with high-permittivity cores [14]. However, the situation is different if the core material does not have such a high permittivity, as is the case with NiZn ferrites [13]. In this scenario, the total capacitive coupling through the core should be much lower, and consequently the total EPC of an inductor or a CMC could instead be determined by C_{tt}. Under these circumstances, it is expected that the use of a loose winding decreases the coupling between two windings of the same coil.

The approach proposed here to validate the hypotheses formulated in the previous paragraph is to construct accurate circuit models of CMCs with different core types and then study the impact of different winding configurations (chiefly tight or loose windings) on the whole model and, more specifically, on its parasitic capacitances. In addition, the actual improvements offered by optimum winding configurations can be quantified by measurements of the transmission coefficients (or insertion loss) of these CMCs in suitable setups.

To perform this analysis, in this work we will use an accurate high-frequency model of the CMC, which is shown in Fig. 2. This circuit model, referred to as modal-parameters circuit (MPC) model of the CMC, was previously proposed in Ojeda-Rodríguez et al.'s [16] work along with an efficient characterization technique that allows quick and simple estimation of the parameters of the MPC model. In Ojeda-Rodríguez et al.'s [16] work, it is demonstrated that due to the symmetry exhibited by a CMC, its equivalent four-ports circuit necessarily has four predetermined natural modes (or eigenvectors of the admittance matrix). These natural modes are referred to as modes G, C, D, and W, and are given in this same order as the columns of the following matrix, which represent the normalized voltage excitations at the corresponding terminals defined in Fig. 2:

$$\boldsymbol{M_m} = \frac{1}{2}\begin{bmatrix} 1 & 1 & 1 & 1 \\ 1 & -1 & -1 & 1 \\ 1 & 1 & -1 & -1 \\ 1 & -1 & 1 & -1 \end{bmatrix}. \tag{1}$$

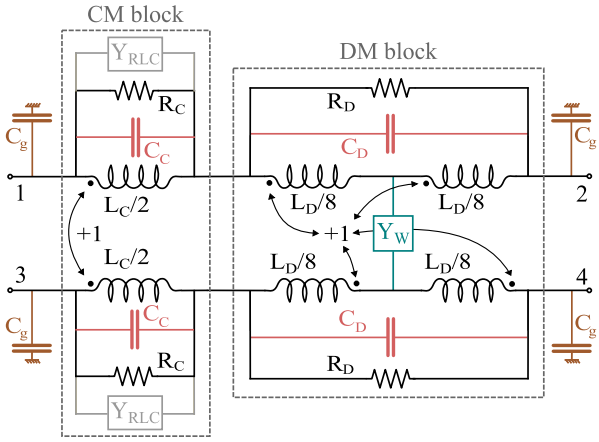

Fig. 2. High-frequency MPC model of a CMC used in this work. The CM and DM blocks determine the response of the component to asymmetrical and symmetrical test setups defined in CISPR-17 standard, respectively [16].

TABLE I
MODAL ADMITTANCES OF THE MPC MODEL OF A CMC

Mode	Admittance
G	$Y_{\mathrm{G}} = j\omega C_g \approx 0$
W	$Y_{\mathrm{W}} = \dfrac{1}{\dfrac{1}{j\omega C_{\mathrm{W}}} + \dfrac{1}{Y_{\mathrm{LCR_W}}}}$
C	$Y_{\mathrm{C}} = Y_{\mathrm{G}} + 2\left(j\omega C_{\mathrm{C}} + \dfrac{1}{j\omega L_{\mathrm{C}}} + \dfrac{1}{R_{\mathrm{C}}} + Y_{\mathrm{RLC}}\right)$
D	$Y_{\mathrm{D}} = 2\left(j\omega C_{\mathrm{D}} + \dfrac{1}{j\omega L_{\mathrm{D}}} + \dfrac{1}{R_{\mathrm{D}}}\right)$

The response of the CMC to each of these four excitations is characterized by modal admittances Y_{G}, Y_{C}, Y_{D}, and Y_{W}, which represent the eigenvalues of the admittance matrix of the CMC. Each modal admittance in the system is composed of various MPC parameters. Although the MPC parameters are primarily modal in nature, they still offer insights into physical aspects of the system. For instance, C_{D} represents the EPC exhibited by the CMC under a differential connection, while C_{W} denotes the parasitic capacitance existing between the coils. It is worth noting that each component within the MPC model contributes only to a specific modal admittance. The modal admittances Y_{C} and Y_{D} account, respectively, for the resonant response of the CMC to CM and DM excitations, while Y_{W} represents capacitive interwinding admittance ($Y_{\mathrm{W}} = j\omega C_{\mathrm{W}}$ as a first approximation) and Y_{G} represents a possible capacitive coupling to ground that can be disregarded in most practical cases [16]. Expressions for these modal admittances in terms of the elements of the MPC model are provided in Table I for the sake of completeness.

The optimization of the winding configuration of a CMC aims to increase the attenuation provided by the CMC to both DM and CM noise. In this work, these attenuations will be measured by using the asymmetrical and symmetrical setups proposed in the CISPR-17 norm, intended to measure the insertion loss of four-ports filtering devices for, respectively, CM and DM [17].

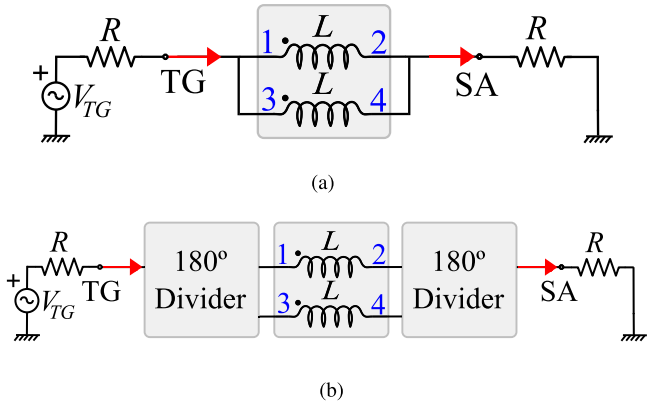

Fig. 3. Setups for characterizing a CMC according to CISPR-17 standard [17] with a spectrum analyzer featuring a tracking generator. (a) CM or asymmetrical-mode setup. (b) DM or symmetrical-mode setup.

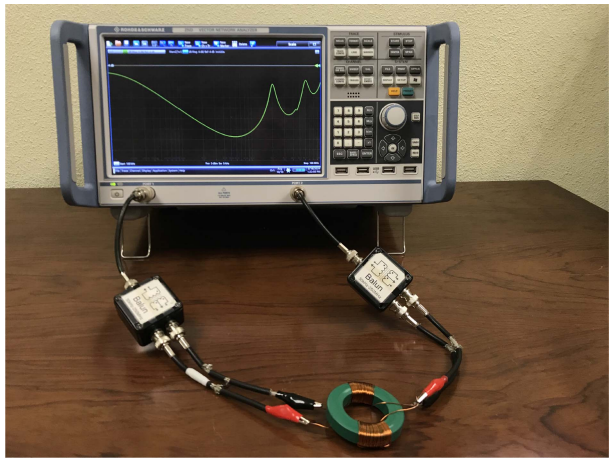

Fig. 4. Setup for insertion loss measurement in symmetrical (DM) connection according to CISPR-17 standard. Commercially available 1:1 transformers (Coilcraft WB2010-1) have been utilized as 180° dividers.

The asymmetrical setup is shown in Fig. 3(a), and is devised to measure the attenuation of CM noise. The symmetrical setup is intended to provide a measure of the attenuation of the DM noise and it is shown in Fig. 3(b). A picture of this setup is provided in Fig. 4. The measurements obtained using these setups are typically accurate up to frequencies in the range of several tens of megahertzs [16], [18], effectively covering the spectrum where most EMC standards establish limits on conducted emissions. Extending measurements to even higher frequencies necessitates the use of specialized test fixtures [19].

In the case of a CMC, the transmission coefficients for the symmetrical and asymmetrical connections can be expressed in terms of the modal admittances of the MPC circuit of the CMC as follows [16]:

$$S_{21}^{\mathrm{asym}} = \frac{2R(Y_{\mathrm{C}} - Y_{\mathrm{G}})}{(2RY_{\mathrm{C}} + 1)(2RY_{\mathrm{G}} + 1)} \tag{2}$$

$$S_{21}^{\mathrm{sym}} = \frac{2R(Y_{\mathrm{D}} - Y_{\mathrm{W}})}{(RY_{\mathrm{D}} + 2)(RY_{\mathrm{W}} + 2)}. \tag{3}$$

Since Y_{G} accounts for a stray capacitance to ground that in most cases is quite small ($Y_{\mathrm{G}} \ll Y_{\mathrm{C}}$), (2) simply indicates that a low

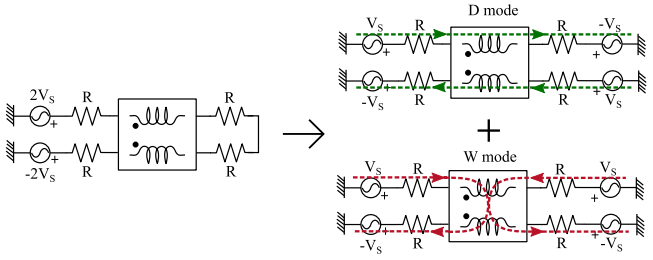

Fig. 5. Equivalent circuit of a CMC connected in symmetrical test setup (left). Decomposition of the circuit into the natural modes excited by the connection. The arrows indicate the direction of the current (right).

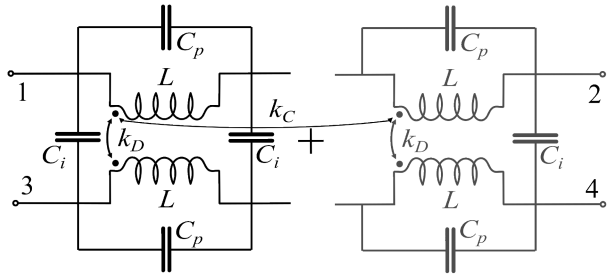

Fig. 6. High-frequency circuit in stages to include distributed effects of CMCs. Each stage is connected in series.

Y_{C} admittance of the CMC will significantly attenuate the CM noise, as expected. Therefore, with respect to attenuation of the CM noise, optimization of the winding strategy of the CMC should be aimed at reducing the parasitic capacitance between turns (C_{C} within Y_{C} in Table I).

Regarding the attenuation of the DM noise, (3) reveals that both the D and W natural modes of the CMC are actually excited in the symmetrical setup. Furthermore, S_{21}^{sym} is proportional to the difference between the corresponding modal admittances, $Y_{\mathrm{D}} - Y_{\mathrm{W}}$. This means that this transmission coefficient could be reduced by ensuring a small value for the parasitic capacitances, but also by adjusting the design of the CMC in such a way that the contributions of Y_{D} and Y_{W} cancel each other out. According to the expressions for Y_{W} and Y_{D} provided in Table I, both Y_{D} and Y_{W} are in principle capacitive at high frequencies. However, Y_{W} may present a resonant behavior, which is accounted for in the MPC model by a $Y_{\mathrm{LCR_W}}$ admittance (a resonant LCR block [16]). Therefore, the condition $Y_{\mathrm{D}} \simeq Y_{\mathrm{W}}$ (optimum DM attenuation) can be reached at high frequencies by ensuring that $2C_{\mathrm{D}} \simeq C_{\mathrm{W}}$, but only within a frequency range where Y_{W} does not resonate ($Y_{\mathrm{LCR_W}} \gg \omega C_{\mathrm{W}}$).

The conditions required for the realizability of the cancellation condition ($Y_{\mathrm{D}} \simeq Y_{\mathrm{W}}$) will be analyzed in Section II-A. Before, it is interesting to briefly explain the physical meaning of this special condition. To do this, it is illustrative to consider Fig. 5, which shows a schematic of the equivalent circuit of a CMC excited according to the symmetrical setup of CISPR-17. Using the superposition principle, this schematic can be decomposed as the sum of the two schematics shown on the right side of the figure, which correspond to excitations of the CMC in mode D (above) and mode W (below). This decomposition reveals that the currents associated with each of these two modes have opposite phases at the output ports of the CMC. Therefore, a fairly small transmission coefficient will be measured when the modal admittances Y_{D} and Y_{W} are quite similar. This means that, under this cancellation condition, the currents associated with two different parasitic capacitive effects are mutually canceling at the output of the CMC.

A. Realizability of the Cancellation Condition

As we will see in Section III, the $2C_{\mathrm{D}} \simeq C_{\mathrm{W}}$ condition can hardly be met in CMCs with MnZn cores due to the high permittivity of the MnZn material [14]. On the contrary, in CMCs with NiZn cores, the capacitances C_{W} and C_{D} are typically of the same order. This makes it possible to achieve the cancellation condition $2C_{\mathrm{D}} \simeq C_{\mathrm{W}}$ by adjusting the angular coverage of the windings. However, in practice, it should be expected that the cancellation condition is maintained only up to a certain frequency due to the resonant behavior of Y_{W}. The resonant behavior of the W mode induces a transition from its capacitive nature to an inductive response, thereby posing a limit to the frequency range where the cancellation effect can be reached. Thus, the question arises as to what extent it is possible to expand the range of frequencies where the W-mode of the CMC is purely capacitive so that the cancellation effect can be maintained in a significant frequency band. This amounts to asking whether resonances of the W-mode are unavoidable or at least can be relegated to a very high frequency.

To answer this question, it is necessary first to identify and characterize the physical mechanism that causes the resonant behavior of the modal admittance Y_{W} of the CMC. In Ojeda-Rodríguez et al.'s [16] work, this is attributed to internal resonances between turns or sections of the CMC windings. A method to verify this hypothesis is to construct a circuit model that accounts for this effect. This model would also allow us to forecast the resonance frequencies of the W-mode of the CMC.

A circuit model of the CMC capable of accounting for the high-frequency resonances of its W-mode should consider both electrical and magnetic couplings between turns of the CMC coils as distributed effects. To construct such a model, we can adapt the approach employed to model distributed inductances and capacitances in transmission line theory [20]. The idea is to progressively split the coils into interconnected subsections. This is illustrated in Fig. 6. That figure includes a first simple single-stage lumped-elements circuit model of the CMC to which stages can be added in series. In that circuit model, capacitances C_p account for the electric coupling between turns of the same coil, whereas capacitances C_i model electric couplings between turns of the two coils. Also, the coupling coefficients k_C and k_D account for magnetic coupling between turns of the same coil or between turns of different coils, respectively. Note that for this coil system to be physically feasible, the constraint $k_C > k_D$ must be satisfied [21].

Since the multistage model proposed in Fig. 6 is passive and reciprocal, it exhibits the same natural modes as the MPC model [16], which allows one to easily establish equivalences between the parameters of this model and those of the MPC model in Fig. 2 so that they exhibit identical behaviors at low

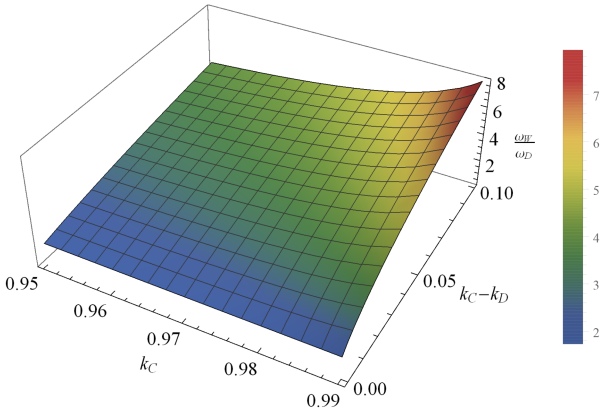

Fig. 7. Ratio between the frequencies of resonance of modes W and D as function of close and distant coupling coefficients. Cancellation of D and W modal capacitances has been assumed.

frequency. For example, for the single-stage circuit, the following relations are obtained: $C_p = C_\mathrm{D} - \frac{C_\mathrm{W}}{2}$ and $C_i = \frac{C_\mathrm{W}}{2}$, $L_\mathrm{D} = L(1 - k_D)$, $L_\mathrm{C} = L(1 + k_D)$.

Taking into account the above-mentioned equivalences, it is found that the single-stage model shows a single resonance for the D mode and none for the W mode, as does the MPC model. This is to be expected because both models neglect the effects of distributed couplings. However, the resonant behavior of Y_W can be straightforwardly reproduced by adding a second stage to the circuit in Fig. 6. To preserve the consistency of this two-stages circuit with the MPC model of the CMC, the following relationship between the parameters must be ensured: $C_p = 2\,C_\mathrm{D} - C_\mathrm{W}$, $C_i = \frac{C_\mathrm{W}}{3}$, $L_\mathrm{D} = 2\,L(1 - 2k_D + k_C)$, and $L_\mathrm{C} = 2\,L(1 + 2k_D + k_C)$. Taking these relationships into account, the following expressions can be obtained for the resonance frequencies of the D and W modes:

$$\omega_\mathrm{res}^D = \sqrt{\frac{3}{(6\,C_\mathrm{D} - C_\mathrm{W})\,(1 - 2\,k_D + k_C)\,L}} \tag{4}$$

$$\omega_\mathrm{res}^W = \frac{3}{\sqrt{(18\,C_\mathrm{D} - 7\,C_\mathrm{W})\,(1 - k_C)\,L}}. \tag{5}$$

If the cancellation condition is assumed in these expressions (i.e., $2C_\mathrm{D} = C_\mathrm{W}$), the ratio $\omega_\mathrm{res}^W/\omega_\mathrm{res}^D$ can be written as follows:

$$\frac{\omega_\mathrm{res}^W}{\omega_\mathrm{res}^D} = \sqrt{3\,\frac{1 - 2\,k_D + k_C}{1 - k_C}}. \tag{6}$$

Note that this ratio depends exclusively on the coupling coefficients k_C and k_D. Because k_C is the coupling coefficient between two adjacent turns of the same coil wound on a core with a high permeability with respect to air, this coefficient should be close to 1.0, while k_D should be slightly below this value. Taking this into account, Fig. 7 shows the ratio $\omega_\mathrm{res}^W/\omega_\mathrm{res}^D$ in (6) represented for a range of possible values of these coupling coefficients. In this figure, it can be seen that $\omega_\mathrm{res}^W/\omega_\mathrm{res}^D$ is between $\sqrt{3}$ and 10. Therefore, the range of frequencies where the CMC can offer very high attenuation for DM noise currents cannot be expected to be greater than a decade. Also, note that k_C and k_D depend on the arrangement of the turns of the windings on the core, just like C_D and C_W. Hence, adjusting the coverage of the core windings to satisfy the cancellation condition $2C_\mathrm{D} = C_\mathrm{W}$ automatically determines the values of k_C and k_D, which cannot be further improved.

TABLE II
RING CORES EMPLOYED IN THIS WORK TO CONSTRUCT THE CHOKES

Core #	Manufacturer	Part number	μ_r @10 kHz	Material
1	FAIR-RITE	5977003821	2000	MnZn
2	TDK	B64290L0082X038	8500	MnZn
3	FAIR-RITE	5943003801	800	NiZn

In conclusion, we have found that, in the case of CMCs with low permittivity cores, it is theoretically possible to adjust the angular coverage of the coils to achieve a very high attenuation of DM noise thanks to the cancellation of the effects of parasitic capacitances C_W and C_D. However, because of the unavoidable presence of internal resonances of the CMC, this ideal attenuation only appears in a finite frequency range. An example showing the typical improvement that can be actually achieved in a practical case is provided in Section III.

III. RESULTS

As already stated, the purpose of this work is to identify optimal winding strategies to reduce the EPC of practical CMCs, thus enhancing their performance at high frequencies. With this aim, in this section we will quantify the effect that key design parameters, such as the distance between turns and the electric permittivity of the core have on the parasitic capacitances of single-layer CMCs. To do this, we constructed different CMC samples by using three different cores made of two different ferrite materials: NiZn and MnZn. These cores are listed in Table II and have been chosen because they have similar sizes while exhibiting a wide range of different permeabilities and permittivities. With each one of these cores, we have constructed CMCs with the same number of turns per winding (30 turns) but different winding geometries. Then, we have obtained a high-frequency equivalent circuit of each of these CMCs employing the method reported in Ojeda-Rodríguez et al.'s [16] work and outlined in Section II. This will allow us to compare the parasitic capacitances of those CMC samples. To verify the impact of the different parasitic capacitances on the performance of these CMCs, we have further measured their transmission coefficients in the asymmetrical and symmetrical test setups defined in CISPR17, intended to characterize attenuations of CM noise and DM noise, respectively, provided by a filtering device. Transmission coefficient measurements have been performed with a R&S ZND VNA.

A. Analysis of the Parameters of the High-Frequency Circuits

Table III presents the parameters obtained for the MPC model of the CMC samples analyzed in this work. For each core, we compared two winding techniques: tight and loose windings. Distance between turns is kept to a minimum in tight

TABLE III
PARAMETERS OF THE MPC MODEL OF THE CMCS CHARACTERIZED IN THIS ARTICLE

Manufacturer part number	Winding technique	C_C (pF)	CR in parallel with C_C			L_C (mH)	R_C (kΩ)	C_D (pF)	L_D (μH)	R_D (kΩ)	C_W (pF)	C_{sym} (pF)	LCR_W network		
			N_{CR}	C_1 (pF)	R_1 (kΩ)								L (μH)	C (pF)	R (kΩ)
FAIR-RITE 5977003821	Tight	**4.79**	1	3.79	26	4.37	∞	**4.11**	82.95	∞	**21.11**	-12.89	2.65	6.92	4
	Loose	**5.81**	1	3.88	19	4.23	6510	**7.67**	40.18	100	**33.84**	-18.50	1.62	17.25	1
TDK B64290L0082X038	Tight	**4.28**	1	8.39	60	35.78	129	**2.98**	103.13	∞	**16.00**	-10.04	3.10	5.57	5
	Loose	**5.03**	1	9.09	54	33.06	147	**4.90**	67.72	132	**23.78**	-13.98	2.62	9.02	3
	Spaced	**2.29**	1	10.69	50	32.88	162	**1.52**	81.56	29123	**4.69**	-1.65	9.78	0.21	5
FAIR-RITE 5943003801	Tight	**1.08**	0			1.69	79	**0.85**	109.94	311	**1.14**	0.56			
	Loose	**0.52**	0			1.58	84	**0.30**	60.27	524	**2.03**	-1.43	22.26	0.10	125
	Optimal	**0.91**	0			1.63	79	**0.63**	83.85	327	**1.30**	-0.04	2.78	2.73	23

Key capacitive parameters are highlighted.

configuration, while loose windings are constructed so that angular coverage of each coil is approximately 120°. Also, for one of the MnZn cores (core 2) we have constructed an additional sample with turns separated from the core (spaced). For the NiZn core (core 3) we have checked an additional winding technique, referred to as optimal, whose details will be provided in Section III-C.

A detailed examination of the parameters in Table III for the tight and loose cases allows us to draw interesting conclusions. First, the CM inductance L_C of the CMCs is highly dependent on the permeability, while the winding strategy has a very weak impact on this CM inductance. This should be expected for a ring-core (nongaped) inductor [22]. In contrast, the DM or leakage inductance, L_D, depends on the winding geometries and is relatively independent of the core permeability. In this sense, the behavior of the L_D inductance is more similar to that of a gaped or a rod-core inductor. This can be explained by the fact that this inductance (leakage inductance) is related to magnetic field lines that close their paths outside the ring core [4].

Focusing more specifically on the capacitive elements of the MPC model of these CMCs shown in Table III, note that the C_C, C_D, and C_W parasitic capacitances of the CMCs with MnZn cores are in general much higher than those obtained for the CMCs with an NiZn core, despite the fact that all these CMCs have the same number of turns. This effect is due to the higher electric permittivity of MnZn cores compared to that of NiZn cores. Physically, this means that the displacement currents through the core play a more significant role in the parasitic electric coupling mechanisms for MnZn cores than for NiZn cores, whose coupling mechanism is more affected by direct electric coupling through the air. Specifically, it should be noted that for CMCs with MnZn cores, increasing the turn-to-turn spacing (loose winding) results in an increase in C_C and C_D. This can be explained by the fact that increasing the separation between turns favors the electric coupling between each turn and the core, thus enhancing the predominant coupling mechanism in high-permittivity cores. This is consistent with the findings reported for inductors in Salomez et al.'s [14] work.

Regarding CMCs with NiZn cores, the parameters in Table III show that C_C and C_D for these CMCs are not only significantly lower than for MnZn cores, but are also lower (instead of higher) for loose windings than for tight windings. The fact that electric coupling decreases as the distance between turns increases is consistent with the idea that, in low-permittivity cores, the coupling through the air may be the dominant effect in the electrical coupling between turns. Also, note that the impact of winding geometry on the parasitic capacitances of the CMC is less significant for MnZn cores than for NiZn cores. In the case of the CMC with an NiZn core, the decrease in C_C (which accounts for the EPC of the CMC excited in CM) when converting a tight to a loose winding is 50%, while the increases experienced by C_C in MnZn cores are of the order of 20%.

Separate consideration is warranted for parasitic capacitance C_W, which accounts for the electrical coupling between the two coils of the CMC. It can be observed from the results in Table III that the capacitances C_W are, for each core, higher for CMCs constructed with loose windings than for CMCs with tight windings. This result is also coherent, since increasing the spacing between turns of each coil reduces the average distance between turns of opposing coils, thus increasing the electrical coupling between them.

B. Comparison of Performances of CMC Samples

1) MnZn Cores (Cores 1 and 2): The analysis of the parameters of the MPC model of the CMCs presented in the previous paragraphs supports the primary hypothesis proposed in this study, which is that the effect of a specific winding strategy on the parasitic capacitances of a CMC highly depends on the permittivity of the core.

To analyze the actual impact of the differences found between the parasitic capacitances of the different CMC samples that we have assembled, we have measured the attenuation provided by these CMCs for both CM and DM signals. Fig. 8 shows the magnitude and phase of the measured S_{21} curves for both the asymmetrical and the symmetrical test setups for the two CMCs (tight and loose windings) constructed with core 1 in Table II (the MnZN core with lower permittivity). To verify the precision of the MPC model, calculated S_{21} curves have also been included in these graphs.

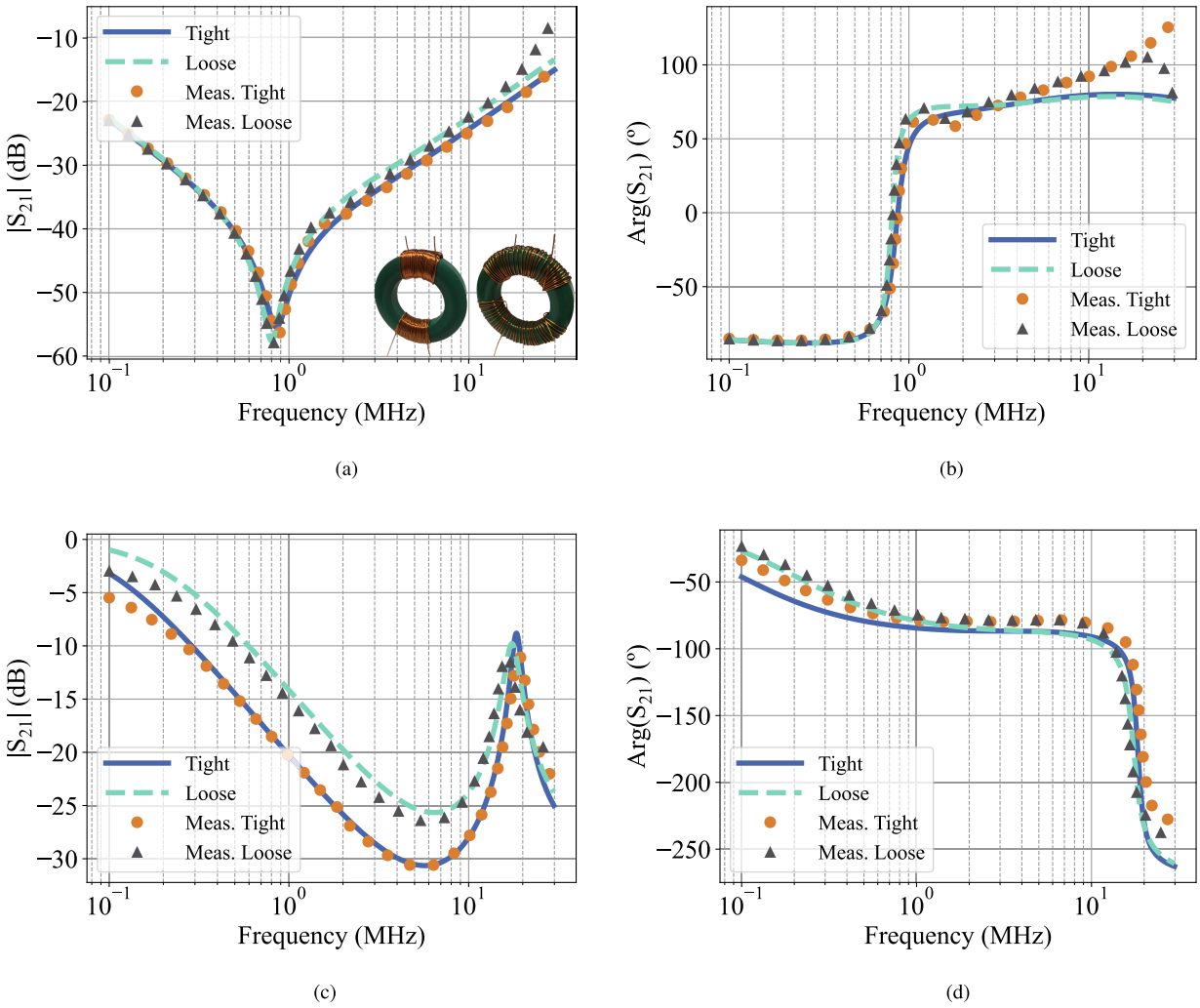

Fig. 8. Transmission coefficients for asymmetrical (CM) and symmetrical (DM) mode connections measured for two samples of 30-turns-per-winding CMCs with tight and loose winding configurations on an MnZn FAIR-RITE 5977003821 core. Measurements are compared with transmission coefficient predicted by the circuit model in Fig. 2 with the parameters given in Table III. Concordances of each pair or experimental and circuit-model curves are quantified by the mean squared errors (MSEs) provided with each description. (a) Asymmetrical mode (CM). Magnitude; MSE$\times 10^{-6}$: Tight: 9.2; Loose: 18. (b) Asymmetrical mode (CM). Phase. (c) Symmetrical mode (DM). Magnitude; MSE$\times 10^{-3}$: Tight: 3.5; Loose: 4.2. (d) Symmetrical mode (DM). Phase.

In Fig. 8(a), it is observed that the tight configuration yields a slight improvement in the attenuation of CM noise at high frequencies compared to the loose configuration. This enhancement is attributed to the fact that the tight-winding configuration reduces the electrical coupling between turns of a CMC with a high-permittivity core. On the other hand, Fig. 8(c) illustrates that the tight configuration also enhances the DM attenuation of the CMC. In this case, the improvement extends to the low-frequency region because, as previously discussed, the reduction in turn-to-turn distances results in an increase in the leakage inductance (L_{D}) of the CMC. In addition, Fig. 8(c) reveals a second high-frequency resonance in the symmetrical transmission coefficient, associated with the resonant behavior of Y_{W}, as discussed in Section II. Fig. 8(b) and (d) depicts the phase of the measured transmission coefficients. It is interesting to observe that these phases exhibit a sharp transition around the resonance frequencies of each coefficient which are accurately captured by the CMC circuit model. These phase transitions are related to changes in the behavior of the modal admittances Y_{C} and Y_{D}. As shown in Table I, these admittances correspond to parallel LCR resonators; hence, they undergo a transition at resonance from an inductive to a capacitive response.

The results for the CMCs constructed with the MnZn core of higher permeability, core 2 in Table II, are represented in Fig. 9. In this case, the higher permeability of the core results in a higher value of L_{C}, resulting in a lower frequency of resonance for S_{21}^{asym}. Otherwise, the conclusions are the same as for the other CMC with the MnZn core: the tight configuration yields slightly better performance than the loose configuration for both CM and DM. This is due to slightly lower parasitic capacitances and higher L_{D}. We conclude that the performance of CMCs with high-permittivity cores cannot be significantly enhanced by changing the turn-to-turn winding distance. The results presented in Salomez et al.'s [14] work for inductors suggest that a more effective strategy to reduce these parasitic capacitances is to increase the distance between the turns and the core. To study the effect of this strategy on the attenuation and on the equivalent circuit of a practical CMC, we have

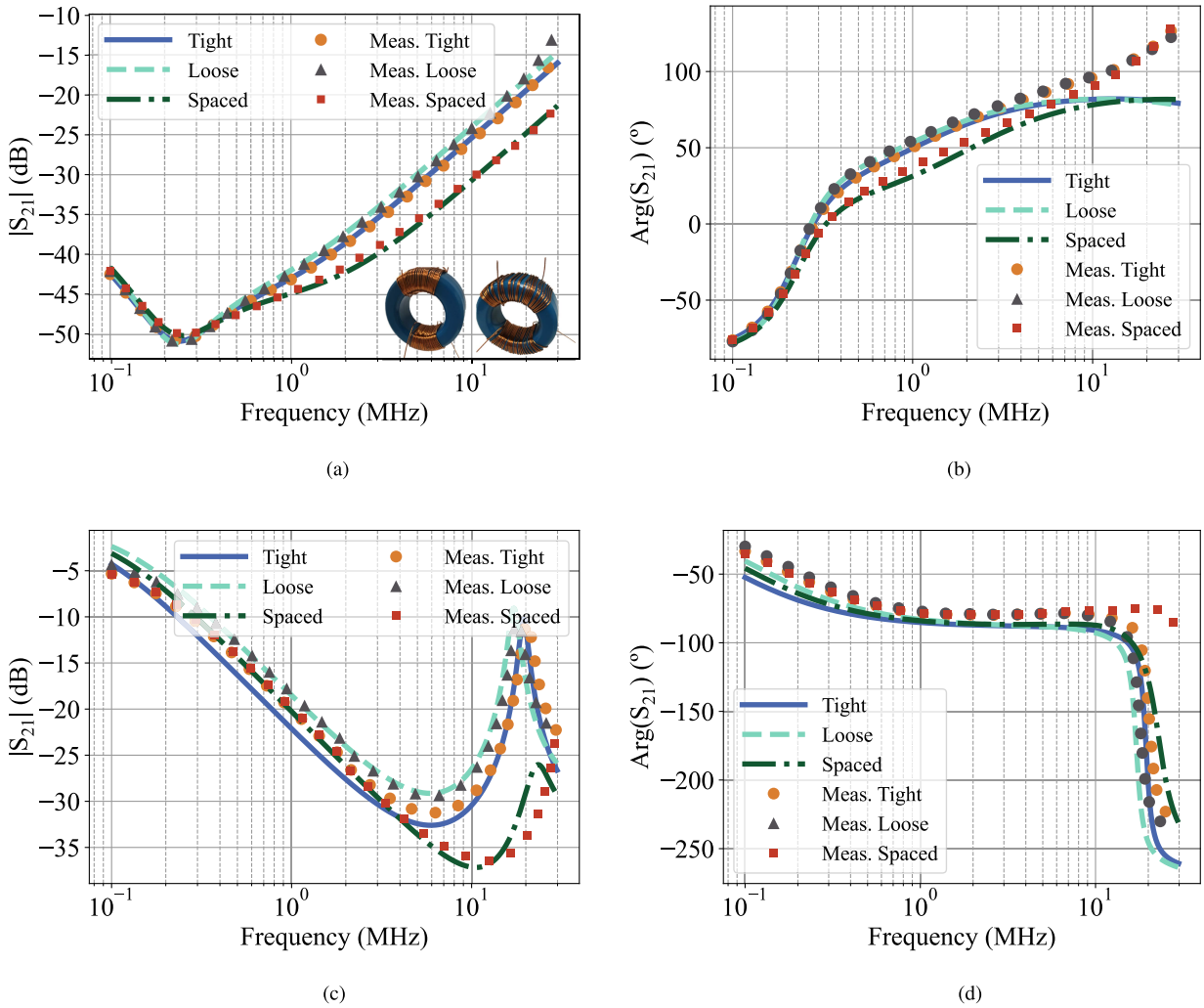

Fig. 9. Transmission coefficients for asymmetrical and symmetrical mode (CM and DM) connections measured for two samples of 30-turns-per-winding CMCs with tight and loose winding configurations on an MnZn TDK B64290L0082X038 core. Measurements are compared with transmission coefficient predicted by the circuit model in Fig. 2 with the parameters given in Table III. Concordances of each pair or experimental and circuit-model curves are quantified by the MSEs provided with each description. (a) Asymmetrical mode (CM). Magnitude; MSE$\times 10^{-6}$: Tight: 6.1; Loose: 9.0; Spaced: 7.1. (b) Asymmetrical mode. Phase. (c) Symmetrical mode (DM). Magnitude; MSE$\times 10^{-3}$: Tight: 1.0; Loose: 3.6; Spaced: 2.9. (d) Symmetrical mode. Phase.

manufactured an additional CMC sample by winding tight coils in the same MnZn core 2. However, the turns of the coils have been separated 2 mm from the core using several layers of low-permittivity insulating material (paper tape). We refer to this winding technique as "Spaced" in Table III, which shows the values of the parameters of the MPC model of this CMC. Note that increasing the space between the turns and the core provides ∼50% reductions in C_{C} and C_{D} parasitic capacitances with respect to the tight version of the CMC, resulting in much better attenuation provided by the CMC at high frequencies for both the symmetrical and asymmetrical mode connections, as shown in Fig. 9. In particular, note the reduction of 5 dBs in CM transmission above resonance. We have verified that similar results can be achieved for the CMC constructed with MnZn core 1. An alternative strategy that could be considered to improve the attenuation of CMCs manufactured with high permittivity cores would be to stack the turns of the windings to separate some of them from the core. However, we have verified that this strategy leads to significant increases in parasitic capacitances C_{C} and C_{D}, resulting in much worse CMC performance at high frequencies.

2) NiZn Core (Core 3): Fig. 10 shows the results obtained for the CMC constructed with the NiZn core identified as core 3 in Table II. Several interesting differences can be observed with respect to the results obtained for MnZn cores. The first difference is that NiZn CMC samples have a significantly lower L_{C} inductance for the same number of turns, as expected. This results in a higher resonance frequency in S_{21}^{asym}, as shown in Fig. 10(a). Moreover, since parasitic capacitances are much lower for this low permittivity core, the attenuation provided at high frequencies is much better than that provided by the CMCs with MnZn cores. However, the most notable difference is that, for the CMC with an NiZn core, the winding configuration that provides better attenuation for CM noise at high frequencies is the loose winding, instead of the tight winding. This agrees with the analysis presented in Section III-A, which concluded that, for low-permittivity cores, increasing the distance between turns should reduce the parasitic capacitance C_{C}.

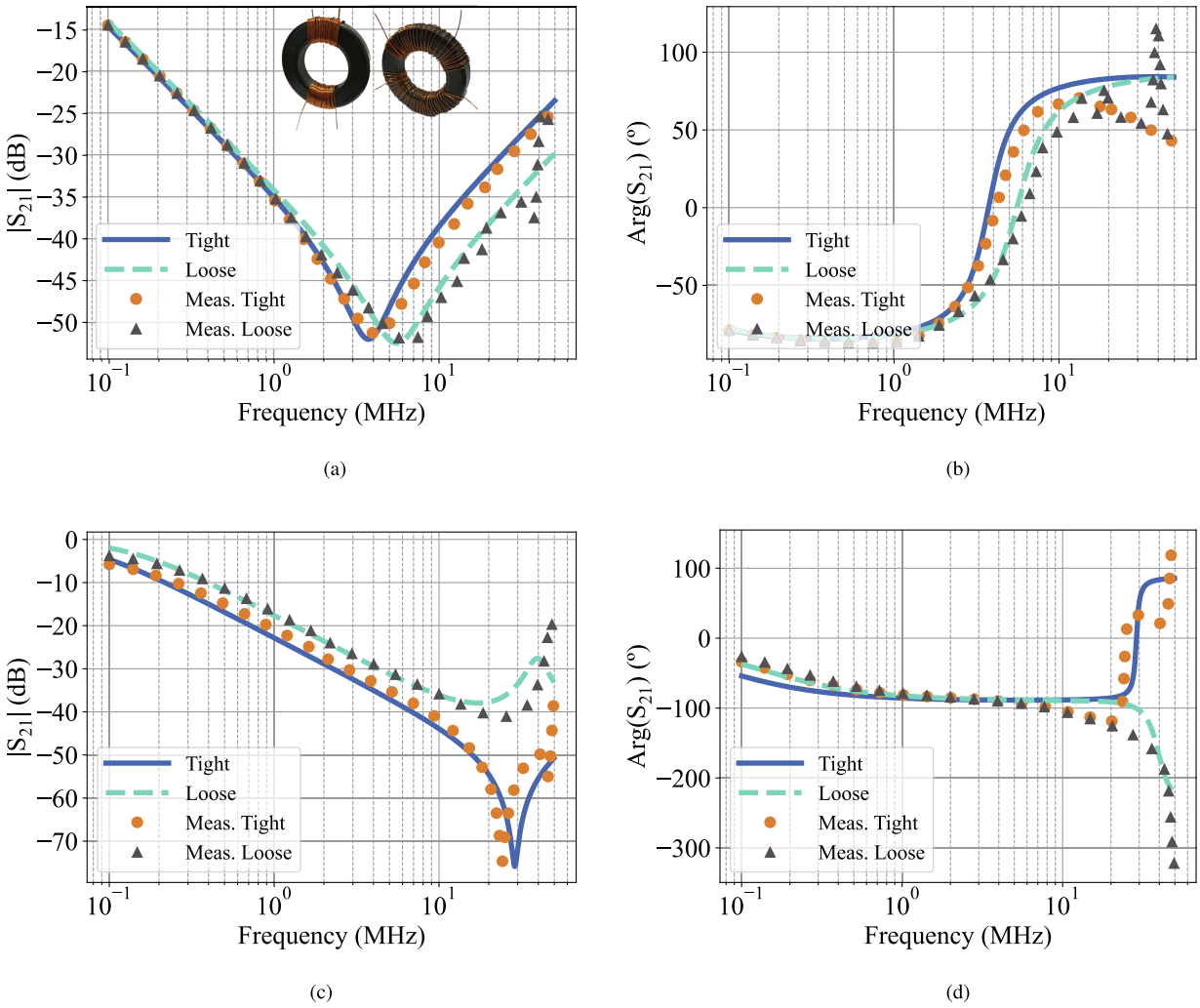

Fig. 10. Transmission coefficients for asymmetrical and symmetrical mode (CM and DM) connections measured for two samples of 30-turns-per-winding CMCs with tight and loose winding configurations on an NiZn FAIR-RITE 5943003801 core. Measurements are compared with transmission coefficient predicted by the circuit model in Fig. 2 with the parameters given in Table III. Concordances of each pair or experimental and circuit-model curves are quantified by the MSEs provided with each description. (a) Asymmetrical mode (CM). Magnitude; MSE$\times 10^{-6}$: Tight: 4.3; Loose: 5.5. (b) Asymmetrical mode. Phase. (c) Symmetrical mode (DM). Magnitude; MSE$\times 10^{-3}$: Tight: 1.5; Loose: 3.4. (d) Symmetrical mode. Phase.

Regarding DM attenuation, the results in Fig. 10(c) show that, similar to high permittivity cores, in this case a higher attenuation is achieved by using the tight configuration, primarily due to its impact on L_{D}. In Fig. 10(c), it can also be observed that the high-frequency behaviors of the transmission coefficient S_{21}^{sym} are markedly different for the loose and tight cases. Specifically, the tight configuration exhibits a sharp resonance, which contrasts with the noticeably smoother resonance of the loose configuration. This is due to the fact that for the loose windings case the condition $C_{\mathrm{W}} > 2C_{\mathrm{D}}$ is met. As a consequence, the difference $Y_{\mathrm{D}} - Y_{\mathrm{W}}$ in the numerator of S_{21}^{sym} in (3) results in a negative total capacitance, preventing the cancellation of susceptances that is necessary for a pronounced resonance. The opposite happens for the tight windings case, where $C_{\mathrm{W}} < 2C_{\mathrm{D}}$. This can be verified by examining the parameters in Table III. What is interesting about this situation is that for this CMC there must exist an intermediate winding arrangement that meets the cancellation condition $C_{\mathrm{W}} \approx 2C_{\mathrm{D}}$. The actual performance of a CMC that satisfies this condition will be investigated in the next section.

C. Customizing DM Attenuation of a CMC With NiZn Core

To construct a CMC whose parasitic capacitances meet the cancellation condition $C_{\mathrm{W}} \simeq 2C_{\mathrm{D}}$, we have constructed an additional single-layer CMC sample with NiZn core (core 3). For this sample, we have started with a tight configuration and have progressively separated the turns of the two coils until a significant change has been observed in the measured transmission coefficient for the symmetrical connection of the CMC. We will refer to this case as the optimal configuration. The parameters of the MPC model corresponding to this optimal case are provided in Table III. Note that $C_{\mathrm{sym}} \simeq 0$ for the optimal case. This means that this sample is quite close to the cancellation condition. The measured curve $|S_{21}^{\mathrm{sym}}|$ for this optimal configuration is compared in Fig. 11 with both the tight

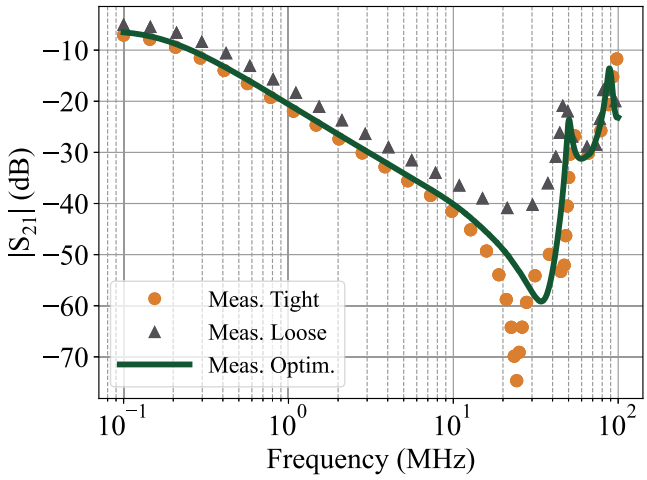

Fig. 11. Measured transmission coefficient in symmetrical connection (DM) for 30-turns per winding CMCs constructed with NiZn FAIR-RITE 5943003801 core. Previous samples with the same core are compared with an additional CMC designed to optimize the gap between neighboring turns.

and the loose cases. In that figure, it can be observed that, due to the presence of additional resonances at high frequencies, an ideal attenuation is not achievable. These results are consistent with the analysis presented in Section II-A, allowing us to conclude that, for single-layer CMCs with low-permittivity cores, the distance between turns can be customized to achieve a compromise solution that significantly enhances attenuation against DM noise compared to the loose configuration while simultaneously providing better attenuation against CM noise than the tight configuration.

IV. Conclusion

This work investigates the influence of core electrical permittivity and winding arrangement on the high-frequency performance of single-layer ring-core CMCs. We constructed various CMC samples using different core materials and winding techniques, meticulously examining their impact on the parasitic capacitances that determine their high-frequency response. By using an accurate high-frequency circuit model for these CMCs, we precisely quantified the effect of various winding strategies on their performance against CM and DM noise.

Our findings confirm the central hypothesis of this study: the electrical coupling mechanism in CMCs varies significantly depending on whether the core is made of MnZn or NiZn material, owing to their distinct electrical permittivities. Specifically, we observed that CMCs with high-permittivity MnZn cores exhibit dominance of displacement currents through the core, while for CMCs with low-permittivity NiZn cores displacement currents through the air are the dominant effect in the electric coupling mechanism. Consequently, the optimal winding strategy for improving high-frequency response differs between these two core types. For CMCs with high-permittivity cores, tight coil winding configurations prove advantageous, while for substantial CM attenuation improvements, a single-layer configuration with windings separated from the core is preferable. In contrast, NiZn cores benefit from increased spacing between turns to enhance CM attenuation, albeit at the cost of DM attenuation. These conclusions, which constitute the main contribution of this work, are supported by experimental measurements and the coherence found between these measurements and the precise circuit models obtained for the analyzed CMCs.

As an additional contribution, we identified an intermediate optimal configuration for NiZn cores, characterized by the cancellation of parasitic capacitors. However, we demonstrated that the significant increases in DM attenuation achieved with this configuration are primarily limited to the vicinity of the CMC's resonance frequency. This analysis is supported by a novel multistage model of the CMC, which allows for explaining and quantifying the bandwidth limitations of this optimization technique. Nevertheless, it is important to emphasize that this multistages model is not proposed in this work as an alternative to the much simpler MPC model for the characterization of CMCs, but only as a mean to calculate the frequency of the high-frequency resonances observed in real CMCs and to explain its physical meaning.

The potential influence of construction asymmetries in practical CMCs on their high-frequency performance is considered an interesting subject for future research work.

References

[1] B. Zhang and S. Wang, "A survey of EMI research in power electronics systems with wide-bandgap semiconductor devices," *IEEE Trans. Emerg. Sel. Topics Power Electron.*, vol. 8, no. 1, pp. 626–643, Mar. 2020.
[2] C. R. Paul, *Introduction to Electromagnetic Compatibility*, 2nd ed. Hoboken, NJ, USA: Wiley, 2006.
[3] H. W. Ott, *Electromagnetic Compatibility Engineering*, 1st ed. Hoboken, NJ, USA: Wiley, 2009.
[4] M. Nave, "On modeling the common mode inductor," in *Proc. IEEE Int. Symp. Electromagn. Compat.*, 1991, pp. 452–457.
[5] A. Massarini and M. Kazimierczuk, "Self-capacitance of inductors," *IEEE Trans. Power Electron.*, vol. 12, no. 4, pp. 671–676, Jul. 1997.
[6] X. Roboam, B. Sareni, and A. Andrade, "More electricity in the air: Toward optimized electrical networks embedded in more-electrical aircraft," *IEEE Ind. Electron. Mag.*, vol. 6, no. 4, pp. 6–17, Dec. 2012.
[7] J. Chen, M.-k. Nguyen, Z. Yao, C. Wang, L. Gao, and G. Hu, "DC-DC converters for transportation electrification: Topologies, control, and future challenges," *IEEE Electrific. Mag.*, vol. 9, no. 2, pp. 10–22, Jun. 2021.
[8] S. Wang, Z. Liu, and Y. Xing, "Extraction of parasitic capacitance for toroidal ferrite core inductor," in *Proc. IEEE 5th Conf. Ind. Electron. Appl.*, 2010, pp. 451–456.
[9] M. Kovacic, Z. Hanic, S. Stipetic, S. Krishnamurthy, and D. Zarko, "Analytical wideband model of a common-mode choke," *IEEE Trans. Power Electron.*, vol. 27, no. 7, pp. 3173–3185, Jul. 2012.
[10] L. Middelstadt, S. Skibin, R. Dobbelin, and A. Lindemann, "Analytical determination of the first resonant frequency of differential mode chokes by detailed analysis of parasitic capacitances," in *Proc. 16th Eur. Conf. Power Electron. Appl.*, 2014, pp. 1–10.
[11] S. W. Pasko, M. K. Kazimierczuk, and B. Grzesik, "Self-capacitance of coupled toroidal inductors for EMI filters," *IEEE Trans. Electromagn. Compat.*, vol. 57, no. 2, pp. 216–223, Apr. 2015.
[12] G. Dong, F. Zhang, Y. Liu, W. Meng, and C. Xu, "Analytical method for extraction of stray capacitance in single-layer CM chokes," in *Proc. IEEE Energy Convers. Congr. Expo.*, 2019, pp. 3185–3191.
[13] Y. Li and S. Wang, "Modeling and increasing the high-frequency impedance of single-layer Mn-Zn ferrite toroidal inductors with electromagnetic analysis," *IEEE Trans. Power Electron.*, vol. 36, no. 6, pp. 6943–6953, Jun. 2021.
[14] F. Salomez, A. Videt, and N. Idir, "Modeling and minimization of the parasitic capacitances of single-layer toroidal inductors," *IEEE Trans. Power Electron.*, vol. 37, no. 10, pp. 12426–12436, Oct. 2022.
[15] A. Ayachit and M. K. Kazimierczuk, "Self-capacitance of single-layer inductors with separation between conductor turns," *IEEE Trans. Electromagn. Compat.*, vol. 59, no. 5, pp. 1642–1645, Oct. 2017.

[16] A. Ojeda-Rodríguez, J. Bernal-Méndez, and M. A. Martín-Prats, "Modal theory and approach for accurate characterization of common mode chokes," *IEEE Trans. Power Electron.*, vol. 38, no. 9, pp. 10516–10529, Sep. 2023.
[17] CISPR, "Methods of measurement of the suppression characteristics of passive EMC filtering devices," IEC Standard CISPR-17:2011, 2011.
[18] J. B. Mendez, M. J. Freire, and M. A. M. Prats, "Overcoming the effect of test fixtures on the measurement of parasitics of capacitors and inductors," *IEEE Trans. Power Electron.*, vol. 35, no. 1, pp. 15–19, Jan. 2020.
[19] H. Jie et al., "VNA-based fixture adapters for wideband accurate impedance extraction of single-phase EMI filtering chokes," *IEEE Trans. Ind. Electron.*, vol. 70, no. 8, pp. 7821–7831, Aug. 2023.
[20] D. Pozar, *Microwave Engineering*. Hoboken, NJ, USA: Wiley, 2011.
[21] Y. Tokad and M. B. Reed, "Criteria and tests for realizability of the inductance matrix," *IEEE Trans. Amer. Inst. Elect. Engineers, Part I: Commun. Electron.*, vol. 78, no. 6, pp. 924–926, Jan. 1960.
[22] W. G. Hurley and W. H. Wölfle, *Transformers and Inductors for Power Electronics: Theory, Design and Applications*. Hoboken, NJ, USA: Wiley, 2013.

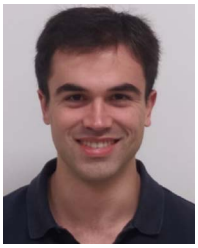

Pablo Ruiz-Morales was born in Seville, Spain, in 2000. He received the master's degree in aeronautical engineering from the University of Seville, Seville, Spain, in 2024. He is currently working toward Ph.D. degree in design and optimization of hybrid electromagnetic interference filters with the Department of Electronic Engineering, University of Seville.

His research focuses on techniques for reducing electromagnetic emissions of power converters for automotive and aeronautical applications.

Álvaro Ojeda-Rodríguez was born in Chipiona, Spain, in 1995. He received the master's degree in aeronautical engineering from the University of Seville, Seville, Spain, in 2019. He is currently working toward the Ph.D. degree in virtual prototyping of passive electromagnetic interference filters with the Department of Electronic Engineering, University of Seville.

He has collaborated in various European and national research projects. His research focuses on modeling and simulating of advanced techniques for mitigation of electromagnetic interference.

Joaquín Bernal-Méndez (Senior Member, IEEE) was born in Seville, Spain, in 1971. He received the Licenciado and Ph.D. degrees from the University of Seville, Seville, Spain, in 1994 and 2000, respectively, both in physics.

In 1995, he joined the Department of Electronics and Electromagnetism, University of Seville. In 1998, he joined the Department of Applied Physics 3, University of Seville, where he became Full Professor in 2024. He has coauthored several patents under exploitation. His research interests include signal integrity and radiation effects in VLSI interconnects, measurement of electromagnetic fields, and electromagnetic compatibility applied to power electronics for aeronautic and space applications.

Dr. Méndez is a Reviewer for IEEE TRANSACTIONS ON MICROWAVE THEORY AND TECHNIQUES, IEEE TRANSACTIONS ON POWER ELECTRONICS, IEEE TRANSACTIONS ON ELECTROMAGNETIC COMPATIBILITY, and IEEE MICROWAVE AND WIRELESS COMPONENTS LETTERS among other international scientific journals.

María A. Martín-Prats (Senior Member, IEEE) received the Licenciado degree in physics and doctoral degree in electronic engineering from the University of Seville, Seville, Spain, in 1996 and 2003, respectively.

In 1996, she joined the Spanish Aerospace Technical National Institute (INTA), where she was with the Renewable Energy Department. In 2000, she joined the Electronic Engineering Department, University of Seville where she became Associated Professor in 2009. Her research interests include avionics and power electronics applied to renewable energy and aerospace applications.

Dr. Prats was the recipient of the Medal of Civil Merit of Spain in 2015 and the Ada Byron Award, in the category of technologist woman, by the University of Deusto, Spain in 2018. She has been a European Coordinator of Universities of the European Defence Agency since 2017 and Member of the Clean Sky Academy working group of the Joint Undertaking of the European Commission since 2017. She has been a Member of the Scientific Committee, advisory group of the Joint Undertaking of the European Commission.